JOURNAL OF GUIDANCE, CONTROL, AND DYNAMICS
Vol. 21, No. 4, July–August 1998

Touch Points in Optimal Ascent Trajectories with First-Order State Inequality Constraints

Sang-Young Park* and Srinivas R. Vadali†
Texas A&M University, College Station, Texas 77843

Two- and three-dimensional optimal ascent trajectories with a dynamic pressure inequality constraint are analyzed for the existence of nontrivial touch points. These studies verify for the first time that such trajectories can have the usual boundary arcs, where the constraint becomes active, as well as *touch points*, which are isolated points where the trajectory touches the constraint boundary. Some of the costates are discontinuous at the touch point. It is also possible to obtain additional insights into the nature of the Lagrange multipliers without solving the optimal control problem, specifically, for the numerical example treated, some of the costate variables can be shown to be zero at a touch point, if it exists.

I. Introduction

NECESSARY conditions for optimal control problems with inequality constraints on the state variables are presented in Refs. 1–5. Extremal trajectories may have different structures depending on the order of the state variable inequality constraint (number of times the constraint has to be differentiated with respect to the independent variable to obtain explicit dependence on a control variable). An extremal trajectory may simply touch the constraint boundary, or it may contain a boundary arc, or it may have both of these structures. It has been shown previously that an extremal trajectory may touch the constraint boundary, but it may not lie along it for constraints of odd orders except the first.[3] Moreover, it has been shown that for first-order state constraints, with additional technical hypothesis, touch points cannot occur.[6,7] The even-order constraint problem is of the touch point type until it eventually turns into the boundary arc type as the constraint is tightened.[6] It is well known that the necessary conditions in Ref. 1 have computational advantages because the state trajectory is held on the state constraint directly by the control.[4] Recently, new necessary conditions for the existence of touch points in the presence of first-order state inequality constraints have been presented.[8]

Because many practical problems involve first-order state variable inequality constraints and numerical methods are dependent on guessing the structures of the optimal trajectories, it is important to investigate the variety of possible structures in detail. Motivated by the work of Ref. 8, in this paper, we analyze theoretically and numerically two- and three-dimensional optimal ascent trajectories with a first-order dynamic-pressure constraint. We consider two aerodynamic models: an artificial model involving constant aerodynamic and moment coefficients and a more realistic model obtained from tabular data. We also consider two classes of flight: trimmed and untrimmed. The solutions obtained by using the multiple shooting method show, for the first time, the existence of touch points in two-dimensional optimal ascent trajectories with dynamic pressure inequality constraints. Three-dimensional optimal ascent trajectories utilizing the two aerodynamic models fail to show the touch point behavior. Additional insight into the nature of the Lagrange multipliers at touch points provided by Ref. 8 have been used to develop special purpose numerical codes to isolate touch points.

Presented as Paper 95-3290 at the AIAA Guidance, Navigation, and Control Conference, Baltimore, MD, Aug. 7–10, 1995; received Dec. 12, 1996; revision received Dec. 20, 1997; accepted for publication Feb. 18, 1998.

*Graduate Student, Department of Aerospace Engineering; currently National Research Council Postdoctoral Associate, Department of Aeronautics and Astronautics, U.S. Naval Postgraduate School, CA 93943. Member AIAA.

†Professor, Department of Aerospace Engineering. Associate Fellow AIAA.

II. Optimality System

We consider the solution of an optimal control problem with two segments (corresponding to the flight of a two-stage rocket) and internal point constraints. A simple optimal control problem can be stated as follows.

Given the performance index

$$J(\boldsymbol{u}) = \phi(\boldsymbol{x}(t_f), t_f) + \int_{t_0}^{t_f} L(\boldsymbol{x}, \boldsymbol{u}, t)\,\mathrm{d}t \tag{1}$$

subject to the dynamic equations and boundary conditions

$$\dot{\boldsymbol{x}} = \boldsymbol{f}(\boldsymbol{x}, \boldsymbol{u}, t), \qquad \boldsymbol{x}(t_0) \equiv \boldsymbol{x}_0, \qquad \text{and} \qquad t_0 \text{ given} \tag{2}$$

and with free final time t_f, find the control history $\boldsymbol{u}(t)$ to minimize $J(\boldsymbol{u})$ with the prescribed terminal constraints

$$\Theta[\boldsymbol{x}(t_f), t_f] = 0 \tag{3}$$

Here $\boldsymbol{x}(t) \in \boldsymbol{R}^n$ are the state variables, $\boldsymbol{u}(t) \in \boldsymbol{R}^l$ are the control components, and $\Theta \in \boldsymbol{R}^k$. We assume that the functions $L, \phi, \boldsymbol{f}$, and Θ are continuously differentiable with respect to all their arguments. The Hamiltonian function is defined with Lagrange multipliers $\Lambda(t) \in \boldsymbol{R}^n$ as

$$H \equiv L + \Lambda^T \boldsymbol{f} \tag{4}$$

The minimum principle requires that the optimal controls minimize H (Ref. 9):

$$\boldsymbol{u}^*(t) = \min_{\boldsymbol{u} \in \Omega} \arg H(\boldsymbol{x}^*, \Lambda^*, \boldsymbol{u}, t) \tag{5}$$

where Ω is the set of admissible piecewise continuous control values and $\boldsymbol{x}^*$, Λ^*, and $\boldsymbol{u}^*$ are the extremal states, costates, and controls, respectively. In this treatment, we use an open set of admissible control values. The states, costates, and the Hamiltonian satisfy the following conditions:

$$\dot{\boldsymbol{x}}^T = H_\Lambda \tag{6a}$$

$$\dot{\Lambda}^T = -H_{\boldsymbol{x}} \tag{6b}$$

$$\Lambda^T(t_f) = \left(\phi_{\boldsymbol{x}} + \nu^T \Theta_{\boldsymbol{x}}\right)_{t=t_f} \tag{6c}$$

$$H(t_f) = -\left(\phi_t + \nu^T \Theta_t\right)_{t=t_f} \tag{6d}$$

$$0 = H_{\boldsymbol{u}} \tag{6e}$$

where ν is a constant multiplier vector of the dimension of the constraint Θ and subscripts indicate partial derivatives. Unless explicitly stated, it is assumed that the Hamiltonian is regular, i.e., Eq. (6e) determines the control uniquely.

State variable inequality constraints are augmented to the cost function, and additional necessary conditions are obtained as a result.[1,3] These necessary conditions, depending on the type of inequality constraint, might require jumps in the costates or the Hamiltonian. Thus, a general optimal control problem requires the solution of a multipoint boundary value problem.

The first-order state inequality constraint is represented as

$$S(\boldsymbol{x}(t)) \equiv q(\boldsymbol{x}) - q_{\max} \leq 0, \qquad 0 \leq t \leq t_f \tag{7}$$

Here $S: \boldsymbol{R}^n \to R$, and q is the dynamic pressure. An extremal trajectory is composed of two types of arcs, interior arcs ($S(\boldsymbol{x}) < 0$) and boundary arcs ($S(\boldsymbol{x}) = 0$) (Ref. 10). Except for junction conditions, an interior arc satisfies the same necessary conditions as the unconstrained problem. Along a boundary arc, the inequality constraint becomes an equality constraint. For numerical convenience,[4] we use the necessary conditions in Ref. 1. The modified Hamiltonian with a pth-order state variable inequality constraint is defined as

$$H = L + \boldsymbol{\Lambda}^T \boldsymbol{f} + \eta S^p \tag{8}$$

where

$$\eta = 0, \qquad \text{if} \qquad S < 0 \tag{9a}$$

$$\eta \geq 0, \qquad \text{if} \qquad S = 0 \tag{9b}$$

and S^p is the pth time derivative of S. Here $p = 1$. Necessary conditions on boundary arcs are

$$H_u = L_u + \boldsymbol{\Lambda}^T \boldsymbol{f}_u + \eta S_u^p = 0, \qquad \left(S_u^p \neq 0\right) \tag{10}$$

$$\dot{\boldsymbol{\Lambda}}^T = -L_x - \boldsymbol{\Lambda}^T \boldsymbol{f}_x - \eta S_x^p \tag{11}$$

The beginning and the end of the constrained arcs are denoted by the times t_{en} and t_{ex}, respectively. At the entry point t_{en}, $S^i[\boldsymbol{x}(t_{\text{en}})] = 0$, $i = 0, \ldots, p-1$, yield the following necessary conditions:

$$\boldsymbol{\Lambda}\left(t_{\text{en}}^+\right) = \boldsymbol{\Lambda}\left(t_{\text{en}}^-\right) - \sum_{i=0}^{p-1} \varepsilon_i S_x^i[\boldsymbol{x}(t_{\text{en}})] \tag{12}$$

$$H\left(t_{\text{en}}^+\right) = H\left(t_{\text{en}}^-\right) \tag{13}$$

$$\boldsymbol{\Lambda}\left(t_{\text{ex}}^+\right) = \boldsymbol{\Lambda}\left(t_{\text{ex}}^-\right) \tag{14}$$

$$H\left(t_{\text{ex}}^+\right) = H\left(t_{\text{ex}}^-\right) \tag{15}$$

where ε_i are constant Lagrange multipliers. The subscripts $-$ and $+$, respectively, denote evaluations just before and just after the entry point t_{en} or the exit point t_{ex}. Equation (12) admits discontinuities in the costate variables at the entry point t_{en}. Because the state inequality constraint does not depend on time explicitly, the Hamiltonian is continuous at the entry point t_{en}. The regularity and continuity of the Hamiltonian at t_{en} result in the continuity of the controls $\boldsymbol{u}(t)$ at t_{en}

$$\boldsymbol{u}\left(t_{\text{en}}^-\right) = \boldsymbol{u}\left(t_{\text{en}}^+\right) = \boldsymbol{u}_b(t_{\text{en}}) \tag{16}$$

We determine the boundary control $\boldsymbol{u}_b$ by using $S^p(\boldsymbol{x}, \boldsymbol{u}) = 0$ over the boundary arcs.[6] Similarly, we have the continuity of $\boldsymbol{u}(t)$ at t_{ex}

$$\boldsymbol{u}\left(t_{\text{ex}}^-\right) = \boldsymbol{u}\left(t_{\text{ex}}^+\right) = \boldsymbol{u}_b(t_{\text{ex}}) \tag{17}$$

For the specific numerical problem considered $S^p = \dot{S}$ is dependent on only one of the free control variables. In such a case, Eq. (10) yields the multiplier $\eta(t)$ explicitly on the boundary arc for a scalar control, along the optimal trajectory, as $\dot{S}_u$ is not zero,

$$\eta(t) = \frac{-\left(L_u + \boldsymbol{\Lambda}^T \boldsymbol{f}_u\right)}{\dot{S}_u} \tag{18}$$

The exit time t_{ex} can be obtained by using Eq. (17). We use the control $\boldsymbol{u}(t)$ from Eq. (6e) on the interior arcs. On boundary arcs, Eqs. (6a) and (11) are the equations of state and costate variables, respectively.

For the extremal arc touching the boundary at a single point, we obtain, for a first-order state constraint, the following necessary conditions[6]:

$$\dot{\boldsymbol{\Lambda}}^T = -L_x - \boldsymbol{\Lambda}^T \boldsymbol{f}_x \tag{19}$$

$$L_u + \boldsymbol{\Lambda}^T \boldsymbol{f}_u = 0 \tag{20}$$

$$S[\boldsymbol{x}(t_{\text{en}})] = 0, \qquad \dot{S}[\boldsymbol{x}(t_{\text{en}})] = 0 \tag{21}$$

$$\boldsymbol{\Lambda}^{+T} = \boldsymbol{\Lambda}^{-T} - \varepsilon_0 S_x \tag{22}$$

We also use the condition $\boldsymbol{u}(t_{\text{en}}) = \boldsymbol{u}_b(t_{\text{en}})$, which is obtained from Eq. (20) and the second of Eqs. (21). From Eqs. (19–22), we notice that the assumption of $S_u^p \neq 0$ is not required for touch point problems.

III. Additional Necessary Conditions at Touch Points

In this section we use the necessary conditions developed in Sec. II and review for completeness additional necessary conditions derived in Ref. 8. The trivial touch point case (unconstrained case, $\varepsilon_0 = 0$) is not treated. When $L = 0$, the modified Hamiltonian on first-order boundary arcs is defined by

$$H = \boldsymbol{\Lambda}^T \boldsymbol{f} + \eta \dot{S}, \qquad \eta \geq 0 \tag{23}$$

and on interior arcs is defined by

$$H = \boldsymbol{\Lambda}^T \boldsymbol{f} \tag{24}$$

The necessary conditions at the entry point (t_{en}) including a touch point are Eqs. (21) and (22).

Theorem: The following is a necessary condition at a touch point for first-order state inequality constraints:

$$\dot{S}_u|_{\boldsymbol{x}^*, \boldsymbol{u}^*} = 0$$

where $\boldsymbol{x}^*$ and $\boldsymbol{u}^*$ indicate the extremal state and control, respectively. This necessary condition can be inferred from the results presented in Ref. 8. Here, we derive the same using Eqs. (20–22).

Proof: With the continuity of the state and control variables at junction points, we have

$$\boldsymbol{f}^- = \boldsymbol{f}^+ \tag{25}$$

where $\boldsymbol{f}^-$ and $\boldsymbol{f}^+$ indicate evaluations of $\boldsymbol{f}$ just before and just after the touch point, respectively. Because $\boldsymbol{f}$ is continuously differentiable with respect to all its arguments, and the controls are continuous at junction points, we obtain

$$\boldsymbol{f}_u^- = \boldsymbol{f}_u^+ \tag{26}$$

Just before and after a touch point, the optimality conditions are

$$\boldsymbol{\Lambda}^{-T} \boldsymbol{f}_u^- = 0 \tag{27a}$$

$$\boldsymbol{\Lambda}^{+T} \boldsymbol{f}_u^+ = 0 \tag{27b}$$

Using Eqs. (22) and (27a), we have

$$0 = \boldsymbol{\Lambda}^{-T} \boldsymbol{f}_u^- = \left(\boldsymbol{\Lambda}^+ + \varepsilon_0 S_x\right) \boldsymbol{f}_u^- \tag{28}$$

From Eqs. (27b) and (28), we obtain the following:

$$\boldsymbol{\Lambda}^{+T} \boldsymbol{f}_u^- + \varepsilon_0 S_x^T \boldsymbol{f}_u^- = 0 = \boldsymbol{\Lambda}^{+T} \boldsymbol{f}_u^+ \tag{29a}$$

$$\boldsymbol{\Lambda}^{+T} \left(\boldsymbol{f}_u^- - \boldsymbol{f}_u^+\right) + \varepsilon_0 S_x^T \boldsymbol{f}_u^- = 0 \tag{29b}$$

Combining Eq. (29b) with Eq. (26), we get

$$\varepsilon_0 S_x^T \boldsymbol{f}_u^- = 0 \tag{30}$$

Equation (30) can be simplified considering that we are analyzing a nontrivial touch point, i.e., $\varepsilon_0 \neq 0$. Thus,

$$S_x^T f_u^- = 0 \tag{31}$$

Note that S and S_x contain neither the control variables nor time, explicitly. Thus, Eq. (31) is equivalent to

$$\frac{\partial}{\partial \boldsymbol{u}}\left(\frac{\partial S}{\partial \boldsymbol{x}}\frac{\mathrm{d}\boldsymbol{x}}{\mathrm{d}t}\right)\bigg|_{t=t^-} = \dot{S}_u^- = 0 \tag{32}$$

Similarly, we obtain

$$0 = \Lambda^{+T} f_u^+ = \left(\Lambda^- - \varepsilon_0 S_x\right)^T f_u^+ \tag{33a}$$

$$\Lambda^{-T}\left(f_u^+ - f_u^-\right) - \varepsilon_0 S_x^T f_u^+ = 0 \tag{33b}$$

$$\dot{S}_u^+ = 0 \tag{34}$$

Equations (32) and (34) at a touch point can be compactly written as

$$\dot{S}_u|_{x^*,u^*} = 0 \tag{35}$$

Lemma: The following conditions are implied at a touch point:

$$\Lambda^{-T} f_u^+ = \Lambda^{-T} f_u^- = \Lambda^{+T} f_u^+ = \Lambda^{+T} f_u^- = 0$$

This lemma is similar to that presented in Ref. 8.

Proof: We obtain, from Eq. (22),

$$\Lambda^{-T} f_u^+ = \left(\Lambda^+ + \varepsilon_0 S_x\right)^T f_u^+ = \Lambda^{+T} f_u^+ + \varepsilon_0 S_x^T f_u^+ = \Lambda^{+T} f_u^+ + \varepsilon_0 \dot{S}_u^+ \tag{36}$$

Using Eqs. (34) and (36), we have

$$\Lambda^{-T} f_u^+ = \Lambda^{+T} f_u^+ = 0 \tag{37}$$

Similarly, with Eq. (22) we obtain

$$\Lambda^{+T} f_u^- = \left(\Lambda^- - \varepsilon_0 S_x\right)^T f_u^- = \Lambda^{-T} f_u^- - \varepsilon_0 \dot{S}_u^- \tag{38}$$

Combining Eq. (32) with Eq. (38), we have

$$\Lambda^{+T} f_u^- = \Lambda^{-T} f_u^- = 0 \tag{39}$$

With Eqs. (37) and (39), we get

$$\Lambda^{-T} f_u^+ = \Lambda^{+T} f_u^+ = \Lambda^{+T} f_u^- = \Lambda^{-T} f_u^- = 0 \tag{40}$$

It is interesting to note that previous studies[3,4,7] on first-order state variable inequality constraints assume the regularity condition $\dot{S}_u \neq 0$ on $S(\boldsymbol{x}) = 0$ for all time, thus eliminating the occurrence of touch points. The regularity condition is satisfied here by requiring that

$$\varepsilon_0 > 0 \tag{41}$$

IV. Model of the Aerospace Vehicle

The physical model chosen for this study is the advanced launch system (ALS) as used in Ref. 11. The model consists of a core and a booster module assembled in parallel to deliver large payloads into a low Earth orbit. The core contains three engines and the booster has seven engines. The combination of the booster and the core is referred to as the first stage, and the second stage refers to only the core vehicle after burnout and jettison of the booster. The payload is to be inserted into a 80 × 150 nm Earth orbit at perigee. The three-degree-of-freedom (three-dimensional) equations of motion relative to the Earth are

$$\dot{\lambda} = \frac{V\cos\gamma\cos\psi}{r\cos\tau} \tag{42a}$$

$$\dot{\tau} = \frac{V\cos\gamma\sin\psi}{r} \tag{42b}$$

$$\dot{h} = V\sin\gamma \tag{42c}$$

$$\dot{V} = (1/m)[T\cos(\alpha+\delta) - D - mg\sin\gamma] + r\omega^2\cos\tau[\cos\tau\sin\gamma - \sin\tau\cos\gamma\sin\psi] \tag{42d}$$

$$\dot{\gamma} = \frac{1}{mV}\{[T\sin(\alpha+\delta)+L]\cos\mu - mg\cos\gamma\} + \frac{V\cos\gamma}{r} + 2\omega\cos\tau\cos\psi + \frac{r\omega^2}{V}\cos\tau[\cos\tau\cos\gamma + \sin\tau\sin\gamma\sin\psi] \tag{42e}$$

$$\dot{\psi} = -\frac{1}{mV\cos\gamma}[T\sin(\alpha+\delta)+L]\sin\mu - \frac{V}{r}\tan\tau\cos\gamma\cos\psi + 2\omega[\cos\tau\tan\gamma\sin\psi - \sin\tau] - \frac{r\omega^2}{V\cos\gamma}\cos\tau\sin\tau\cos\psi \tag{42f}$$

$$\dot{m} = -\frac{c}{I_{\mathrm{sp}} g_s} T_{\mathrm{vac}} \tag{42g}$$

where λ is the longitude, τ is the latitude, h is the altitude above mean sea level, V is the velocity, γ is the flight-path angle, ψ is the heading angle, m is the mass, $r = r_s + h$ is the distance from the center of the Earth to the vehicle center of gravity, ω is the angular velocity of the Earth, D is the drag, L is the lift, T is the thrust, I_{sp} is the specific impulse, and c is the number of engines operating. The control variables are the gimbal angle of the thrust vector, δ, the angle of attack α, and the velocity roll angle μ. With regard to signs, a positive roll angle results in a negative heading angle toward the south.

The thrust model is given by

$$T = c[T_{\mathrm{vac}} - pA_e] \tag{43}$$

where T_{vac} is the thrust of one engine in a vacuum, p is the atmospheric pressure at the current altitude, A_e is the exit area of one engine, and c indicates the number of engines. Density and pressure are modeled as the following exponential functions of altitude:

$$\rho = \rho_s e^{-h/h_1} \tag{44}$$

$$p = p_s e^{-h/h_2} \tag{45}$$

where ρ_s is the density at sea level, p_s is the pressure at sea level, h_1 is the density scale height, and h_2 is the pressure scale height. The Earth is assumed to be a rotating, spherical body with an inverse square gravity field,

$$g = g_s(r_s/r)^2 \tag{46}$$

where g_s is the gravitational force at sea level and r_s is the radius of the Earth at sea level. The speed of sound a is given using the perfect gas law

$$a = \sqrt{\beta(p/\rho)} \tag{47}$$

where β is the ratio of specific heats of air. The dynamic pressure q, the drag D, and the lift L are defined as

$$q = \tfrac{1}{2}\rho V^2 \tag{48}$$

$$D = qA_b C_D \tag{49}$$

$$L = qA_b C_L \tag{50}$$

where A_b is the cross-sectional area, C_D is the drag coefficient, and C_L is the lift coefficient. C_D, C_L, and the pitching moment coefficient C_m are modeled as polynomials in α during the first stage,

$$C_D = C_{D0}(M) + C_{D1}(M)\alpha + C_{D2}(M)\alpha^2 + C_{D3}(M)\alpha^3 \tag{51a}$$

$$C_L = C_{L1}(M)\alpha \tag{51b}$$

$$C_m = C_{m0}(M) + C_{m1}(M)\alpha \tag{51c}$$

where M is Mach number. After staging, the vehicle flies at hypersonic velocities, the aerodynamic force coefficients are assumed to be independent of the Mach number, and pitching moments are assumed to be negligible. The aerodynamic models for the second stage are

$$C_D = C_{D0} + C_{D2}\alpha^2 \tag{52a}$$

$$C_L = C_{L1}\alpha + C_{L2}\alpha|\alpha| \tag{52b}$$

The drag coefficient, the lift coefficient, and the pitching moment coefficient are given in tabular form as functions of Mach number and α in Ref. 12. The sign of C_{L2} depends on the sign of α. It should be noted that during the second stage, the drag coefficient is a symmetric function of α, whereas the lift coefficient is an antisymmetric function of α.

Some restrictions are imposed on the discussed three-dimensional problem to formulate the two-dimensional problem. For the two-dimensional problem, the vehicle is assumed to be launched from the equator, and it remains in the equatorial plane throughout the trajectory. This constrains the latitude, the heading angle, and their corresponding Lagrange multipliers to remain zero throughout the entire trajectory. A nonrotating Earth model is assumed for the two-dimensional problem. Consequently, there are five state variables (the longitude, the altitude, the velocity, the flight-path angle, and the mass) and five corresponding multipliers. The velocity roll angle is assumed to be equal to zero throughout the entire trajectory because there is no motion out of the plane during the flight. The only free control is the angle of attack, and the thrust gimbal angle can be a constrained control, a direct function of α.

In the subsequent sections mention is made of trimmed and untrimmed flights. Trimmed flight refers to the condition of pitching moment balance, achieved by controlling the thrust gimbal angle. The pitching moment is neglected completely for untrimmed flight. Untrimmed flight is considered only to study a simplified problem.

V. Numerical Implementation

We augment the optimality system with additional parameters to determine the switching structure and the final time. The additional parameters are t_{en} and t_{ex}, the constraint boundary entry and exit times, respectively, and t_f, the final time. These parameters are introduced in the following manner.

For the first stage,

$$\dot{t}_{\text{en}} = 0 \qquad \text{and} \qquad \dot{t}_{\text{ex}} = 0 \tag{53a}$$

For the second stage,

$$\dot{t}_f = 0 \tag{53b}$$

The velocity roll angle and the angle of attack are calculated from the optimality conditions, Eq. (10). The optimal control problem is to find the optimal trajectory that maximizes the final mass of the ALS. Thus, the performance index is taken to be $J = -m_f/m_{\text{ref}}$. Here m_f represents the final mass and m_{ref} represents the sum of the masses of the payload, the payload margin, and the payload fairing. The magnitude -1.0 of the performance index indicates that the reference mass is inserted into orbit without any fuel remaining.

The dynamic pressure constraint is imposed as a state inequality constraint by limiting it to $q_{\max}$. This constraint being first order in nature leads to jumps in the altitude and velocity costates. In this section, the analysis of the three-dimensional problem is presented, and the two-dimensional problem can also be treated by the same procedure. The inequality constraint is expressed as follows:

$$S(\boldsymbol{x}) = \tfrac{1}{2}\rho V^2 - q_{\max} \le 0 \tag{54a}$$

where $q_{\max}$ is a constant. We determine the boundary control on the boundary arc using the following equation:

$$\begin{aligned}\dot{S}(\boldsymbol{x}, \boldsymbol{u}) &= -(1/2h_1)\rho V^3 \sin\gamma \\ &+ \rho V[(1/m)\{T\cos(\alpha+\delta) - D - mg\sin\gamma\} \\ &+ r\omega^2\cos\tau\{\cos\tau\sin\gamma - \sin\tau\cos\gamma\sin\psi\}] = 0\end{aligned} \tag{54b}$$

The additional internal boundary conditions are Eqs. (12), (16), (17), and $q(t_{\text{en}}) = q_{\max}$ at the entry and exit point of the boundary arc.

For the ALS problem, there are seven known state variables at t_0 and two known state variables at t_f. Equation (3) includes two boundary equations at final time t_f

$$\begin{aligned}\Theta_1 &\equiv V_f - (V^2 + 2Vr\omega\cos\gamma\cos\psi\cos\tau + r^2\omega^2\cos^2\tau)^{\frac{1}{2}} \\ &= 0\end{aligned} \tag{55a}$$

$$\begin{aligned}\Theta_2 &\equiv \frac{\cos i_f - \cos\tau(V\cos\gamma\cos\psi + r\omega\cos\tau)}{(V^2\cos^2\gamma + 2Vr\omega\cos\gamma\cos\psi\cos\tau + r^2\omega^2\cos^2\tau)^{\frac{1}{2}}} \\ &= 0\end{aligned} \tag{55b}$$

where V_f and i_f are given by the final conditions of the velocity and the inclination, respectively. From the transversality conditions, we obtain $\Lambda_\lambda(t_f) = 0$, $\Lambda_{t_f}(t_f) = 0$, and $\Lambda_m(t_f) = -1/m_{\text{ref}}$, and we also have

$$\Lambda_\tau(t_f) - \nu_1\frac{\partial\Theta_1}{\partial\tau}\bigg|_{t_f} - \nu_2\frac{\partial\Theta_2}{\partial\tau}\bigg|_{t_f} = 0 \tag{56a}$$

$$\Lambda_V(t_f) - \nu_1\frac{\partial\Theta_1}{\partial V}\bigg|_{t_f} - \nu_2\frac{\partial\Theta_2}{\partial V}\bigg|_{t_f} = 0 \tag{56b}$$

$$\Lambda_\psi(t_f) - \nu_1\frac{\partial\Theta_1}{\partial\psi}\bigg|_{t_f} - \nu_2\frac{\partial\Theta_2}{\partial\psi}\bigg|_{t_f} = 0 \tag{56c}$$

where ν_1 and ν_2 are Lagrange multipliers. From Eqs. (56a) and (56b), we can calculate ν_1 and ν_2 as follows:

$$\begin{aligned}\nu_2 = &\left[\Lambda_V(t_f) - \Lambda_\tau(t_f)\frac{\partial\Theta_1}{\partial V}\bigg|_{t_f}\Big/\frac{\partial\Theta_1}{\partial\tau}\bigg|_{t_f}\right]\Big/ \\ &\left[\frac{\partial\Theta_2}{\partial V}\bigg|_{t_f} - \frac{\partial\Theta_2}{\partial\tau}\bigg|_{t_f}\frac{\partial\Theta_1}{\partial V}\bigg|_{t_f}\Big/\frac{\partial\Theta_1}{\partial\tau}\bigg|_{t_f}\right]\end{aligned} \tag{57a}$$

$$\nu_1 = \left[\Lambda_\tau(t_f) - \nu_2\frac{\partial\Theta_2}{\partial\tau}\bigg|_{t_f}\right]\Big/\frac{\partial\Theta_1}{\partial\tau}\bigg|_{t_f} \tag{57b}$$

The preceding two-point boundary problem can be completely solved with these boundary conditions and interior conditions. Because the problem is very sensitive to initial guesses, the multiple shooting method is used with 16 subintervals to reduce the sensitivity. The internal boundary conditions at each subinterval are satisfied by the continuity of state and costate variables in the multiple shooting method.

A special code was also written to isolate touch points. This code was used only when the results of the standard multiple-shooting code indicated possible touch point behavior. In this implementation, the touch point time and the maximum dynamic pressure were determined by imposing the additional necessary conditions required at touch points.

VI. Hodograph Analysis

This section is motivated by the geometric approach to visualize the necessary conditions for the existence of a touch point in Refs. 8 and 13. The hodograph at a given time and state is the set of all possible state rates that can be attained by varying the controls within their allowed domain. Thus, an l-dimensional manifold is generated in the n-dimensional state rate space (for the three-dimensional problem, $n = 7$ and $l = 2$ and for the two-dimensional problem, $n = 5$ and $l = 1$). For the three-dimensional problem under consideration, it suffices to look only at the $\dot{V}$, $\dot{\gamma}$, and $\dot{\psi}$ components of the state rate vectors because the right-hand sides of all other state rates are independent of the controls and, hence, they only trace a single point as the controls are varied. As we are mainly interested in convexity issues, we do not lose any information by visualizing the hodograph in a coordinate system (k_1–k_2–k_3), which is scaled and shifted with

respect to the $\dot{V}$, $\dot{\gamma}$, $\dot{\psi}$ system. The (k_1–k_2–k_3) axes are defined as follows:

$$k_1 = m\dot{V} + mg\sin\gamma - mr\omega^2\cos\tau(\cos\tau\sin\gamma - \sin\tau\cos\gamma\sin\psi) \tag{58a}$$

$$k_2 = mV\left[\dot{\gamma} - \frac{V\cos\gamma}{r} - 2\omega\cos\tau\cos\psi - \frac{r}{V}\omega^2\cos\tau \times (\cos\tau\cos\gamma + \sin\tau\sin\gamma\sin\psi)\right] + mg\cos\gamma \tag{58b}$$

$$k_3 = -mV\cos\gamma[\dot{\psi} + (V/r)\tan\tau\cos\gamma\cos\psi - 2\omega(\cos\tau\tan\gamma\sin\psi - \sin\tau) + r\omega^2\cos\tau\sin\tau\cos\psi/(V\cos\gamma)] \tag{58c}$$

It can also be verified from equations of motion that

$$k_1 \equiv T\cos(\alpha+\delta) - D \tag{59a}$$

$$k_2 \equiv [T\sin(\alpha+\delta) + L]\cos\mu \tag{59b}$$

$$k_3 \equiv [T\sin(\alpha+\delta) + L]\sin\mu \tag{59c}$$

It is obvious from Eqs. (59) that the hodograph in the (k_1–k_2–k_3) system can be obtained by rotating the hodograph in the (k_1–k_2) system about the k_1 axis. The hodograph in the (k_1–k_2) system can be visualized using the following method. Let σ be an auxiliary parameter that varies from -1 to $+1$, boundaries excluded. Then, $\alpha^*(\sigma)$ and $\delta^*(\sigma)$ are calculated by using the following equation:

$$[\alpha^*(\sigma), \delta^*(\sigma)] = \arg\max_{\alpha\in\Omega} Q(\sigma) \tag{60}$$

where Ω is the set of admissible controls, i.e.,

$$\Omega = \{\alpha \in R, \delta \in R \mid \text{pitching moment} = 0\} \tag{61}$$

and

$$Q(\sigma) \equiv \sqrt{1-\sigma^2}[T\cos(\alpha+\delta) - D] + \sigma[T\sin(\alpha+\delta) + L] \tag{62}$$

This procedure equivalently yields the controls $[\alpha^*(\sigma), \delta^*(\sigma)]$ that minimize the Hamiltonian

$$H = \Lambda_{k_1}k_1 + \Lambda_{k_2}k_2 + \Lambda_{k_3}k_3 + \text{terms independent of controls} \tag{63}$$

with $\Lambda_{k_1} = -\sqrt{(1-\sigma^2)}$, $\Lambda_{k_2} = -\sigma$, and $\Lambda_{k_3} = 0$. Note that, as σ is varied, Λ_{k_1} defined earlier remains negative, which is required for the existence of a bounded control. The hodograph in the (k_1–k_2) system is obtained by plotting the curve

$$k_1(\sigma) = T\cos[\alpha^*(\sigma) + \delta^*(\sigma)] - D|_{\alpha^*(\sigma)} \tag{64a}$$

$$k_2(\sigma) = T\sin[\alpha^*(\sigma) + \delta^*(\sigma)] + L|_{\alpha^*(\sigma)} \tag{64b}$$

Rotation of the hodograph in the (k_1–k_2) system about the k_1 axis results in the hodograph in the (k_1–k_2–k_3) system. It should be noted that a necessary condition for convexity of the hodograph is that k_1 is maximized at $k_2 = 0$.

VII. Touch Points in Two-Dimensional Extremals

Artificial Aerodynamic Data

We use the artificial aerodynamic data given in Ref. 14 to create a synthetic aerodynamic model. The drag D and the lift L are defined as

$$D = qA_b(C_a + C_N\alpha^2) \tag{65}$$

$$L = qA_b(C_N - C_a)\alpha \tag{66}$$

where ρ is the density, A_b is the reference area, and α is the angle of attack. The numerical values for C_a and C_N are 0.3 and 3.1, respectively. We note that these constant values for the aerodynamic coefficients are unrealistic; however, this assumption allows us to easily obtain insights into the touch point problem. It is clear from the preceding equations that the derivative of the drag with respect to α is zero and the lift is zero at zero angle of attack,

$$\left.\frac{\partial D}{\partial\alpha}\right|_{\alpha=0} = 2qA_bC_N\alpha = 0 \tag{67a}$$

$$L|_{\alpha=0} = 0 \tag{67b}$$

The time derivative of the dynamic pressure constraint is

$$\dot{S}(\boldsymbol{x},\boldsymbol{u}) = -(1/2h_1)\rho V^3\sin\gamma + \rho V[(1/m)(T\cos\alpha - D) - g\sin\gamma] \tag{68}$$

Because α is a free control and it appears in Eq. (68), we have to deal with a first-order state inequality constraint. Discontinuities in the altitude and velocity costate variables will occur at the entry point t_{en} because the inequality constraint is dependent on only these two state variables.

To visualize the hodograph, it suffices to look only at the $\dot{V}$ and $\dot{\gamma}$ components of the state rate vectors. As already mentioned, we can also visualize the hodograph in the (k_1–k_2) coordinate system, which is scaled and shifted with respect to the $\dot{V}$, $\dot{\gamma}$ system. The (k_1–k_2) axes are defined as follows for the two-dimensional untrimmed flight:

$$k_1 = T\cos\alpha - D \tag{69a}$$

$$k_2 = T\sin\alpha + L \tag{69b}$$

With these assumption and definitions, applicability of the touch point theorem is now investigated. Table 1 shows the results of running the usual optimization code developed for different values of the dynamic pressure constraint indicating a touch point approximately at $q = 721.54$ lb/ft^2. A special purpose multiple shooting code was written for the touch point case, treating the touch point time as a free variable and by imposing the touch point conditions.

Table 1 $\dot{S}_u$ vs q for two-dimensional flight with a synthetic aerodynamic model

q_{max}, lb/ft^2	t_{en}, s	t_{ex}, s	Boundary arc, s	k_2	$\dot{S}_\alpha$
997.225	68.869325103	68.869325327	2.24e−7	1.29812498e+6	−2.51093871e+1
950.0	68.617246952	68.715195050	9.79e−2	1.15884620e+6	−2.14428563e+1
850.0	68.042184351	68.210812916	1.69e−1	7.90523786e+5	−1.32381482e+1
750.0	67.397172721	67.427269296	3.01e−2	2.28745301e+5	−3.43634911e+0
725.0	67.200269477	67.200892386	6.23e−4	3.01552327e+4	−4.40449909e−1
722.0	67.173990785	67.174002202	1.14e−5	4.03901650e+3	−5.87961063e−2
721.58	67.170241353	67.170241434	8.12e−8	3.43958118e+2	−5.00465708e−3
721.545	67.169926283	67.169926283	4.40e−10	3.48300296e+1	−5.06763821e−4
721.536	67.169797164	67.169797165	1.10e−9	−3.20006090e+1	4.65592377e−4
721.5	67.169462791	67.169462838	4.74e−8	−3.54511578e+2	5.15775518e−3
721.0	67.165059781	67.165075892	1.61e−5	−4.78403138e+3	6.95633691e−2
700.0	66.951580355	66.985804379	3.42e−2	−2.04415100e+5	2.90415352e+0
600.0	63.718445275	67.153673311	3.44e+0	−1.37477795e+6	1.82177942e+1

Table 2 $\dot{S}_u$ vs q for two-dimensional flight with realistic aerodynamic model

q_{max}, lb/ft^2	t_{en}, s	t_{ex}, s	Boundary arc, s	k_2	$\dot{S}_\alpha$
679.2	68.213674804	68.213757641	8.28e−5	5.26168715e+5	−8.31980092e+0
660.0	67.632981513	67.658608169	2.56e−2	3.93986092e+5	−6.36089890e+0
620.0	66.366925707	66.369996056	3.07e−3	6.33925428e+4	−1.19002509e+0
614.0	66.166715724	66.166772911	5.72e−5	2.60889714e+3	−1.51403818e−1
613.5	66.151187783	66.151194619	6.84e−6	−2.84462262e+3	−5.81717847e−2
612.5	66.102288645	66.102303955	1.53e−5	−9.42566247e+3	5.51414341e−2
610.0	66.030301881	66.031214276	9.12e−4	−4.00305655e+4	5.78325548e−1
600.0	65.674054231	65.696011474	2.20e−2	−1.54968615e+5	2.54975508e+0
570.0	64.265229494	64.873735985	6.09e−1	−5.82544181e+5	9.92890536e+0

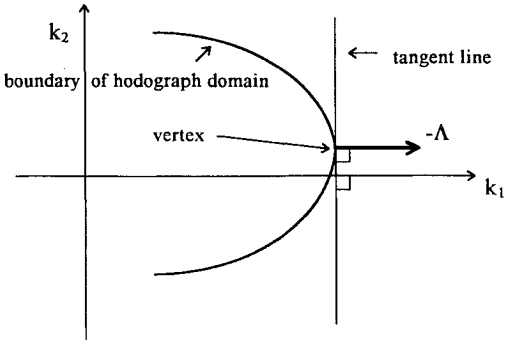

Fig. 1 Hodograph for the two-dimensional problem.

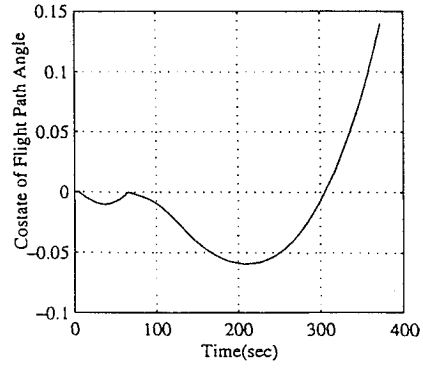

Fig. 2 Λ_γ history for the two-dimensional touch point trajectory.

The results show that at a certain dynamic pressure (approximately, $q = 721.54$ lb/ft^2 at $t = 67.17$ s) the length of the boundary arc, k_2, α, and $\partial\dot{S}/\partial\alpha$ are zero (the touch point). Note that k_2 becomes zero when α is zero. Hence,

$$\frac{\partial \dot{S}}{\partial \alpha} = \frac{\rho V}{m}\left(T\sin\alpha + \frac{\partial D}{\partial \alpha}\right) = 0 \tag{70}$$

Equation (70) indicates that $k_1 = T\cos\alpha - D$ is an extremum with respect to α at a touch point. Therefore, α and k_2 are necessarily zero at the touch point. The optimal control combination is determined by the $k(k_1, k_2)$ vector, which lies in the hodograph domain and has the largest projection on the costate vector. This point picked out by the minimum principle lies on the boundary of the hodograph domain, if the domain is convex. For a given state vector, the minimum principle yields a state rate vector on the convex hull of the hodograph such that the costate vector is perpendicular to the separating tangent plane at this point. As k_1 is maximized at the touch point, the costate vector is parallel to the k_1 axis, as shown in Fig. 1 for two-dimensional problems, regardless of the value of k_2. This means that the costate $\Lambda_{k_2}(\equiv \Lambda_\gamma) = 0$ at the touch point. Thus, the hodograph analysis gives us a clue that Λ_γ is zero at the touch point. The optimality condition is

$$\frac{\partial H}{\partial \alpha} = \frac{-\Lambda_V}{m}\left(T\sin\alpha + \frac{\partial D}{\partial \alpha}\right) + \frac{\Lambda_\gamma}{mV}\left(T\cos\alpha + \frac{\partial L}{\partial \alpha}\right) = 0 \tag{71}$$

Because both $T\sin\alpha + (\partial D/\partial\alpha)$ and Λ_γ are zero at the touch point, the optimality condition, i.e., Eq. (71), is automatically satisfied at the touch point with $\alpha = 0$.

Realistic Aerodynamic Data

Next, we consider trimmed two-dimensional flight. The constrained equations of motion and the aerodynamic data mentioned in Sec. IV are used. The differentiation of the inequality constraint results in

$$\dot{S}(\boldsymbol{x}, \boldsymbol{u}) = -(1/2h_1)\rho V^3 \sin\gamma + \rho V[(1/m)(T\cos(\alpha+\delta) - D) - g\sin\gamma] \tag{72}$$

The (k_1–k_2) axes are defined as follows:

$$k_1 = T\cos(\alpha+\delta) - D \tag{73a}$$

$$k_2 = T\sin(\alpha+\delta) + L \tag{73b}$$

The necessary condition for a touch point is given by the following:

$$\frac{\partial \dot{S}}{\partial \alpha} = \frac{\rho V}{m}\left[T\sin(\alpha+\delta)\left(1 + \frac{\partial \delta}{\partial \alpha}\right) + \frac{\partial D}{\partial \alpha}\right] = 0 \tag{74}$$

Table 2 shows that near $q = 613$ lb/ft^2 indications of a touch point are present. The convergence of the numerical code was not satisfactory near this dynamic pressure limit. The special code yielded the following converged results: $q = 612.71064201$ lb/ft^2 at the touch point at $t = 66.10371976$ s, $k_2 = -6.19059048$e+3, and $\dot{S}_\alpha = 8.187$e−9. Note that k_2 is not zero when k_1 is maximized with respect to α, i.e., $\dot{S}_\alpha = 0$, at the touch point. This results in a nonzero value of the angle of attack at the touch point. As mentioned in the preceding section, regardless of the value of k_2, the costate vector is parallel to the k_1 axis at the vertex of hodograph when k_1 is maximized (Fig. 1). Hence, $\Lambda_\gamma = 0$ at the touch point. As expected, numerical results show that the costate of the flight-path angle is zero at the touch point (Fig. 2), and $\dot{S}$ is maximized over the control domain at the touch point ($\alpha = -0.4376266$ deg), verifying the existence of a touch point.

In summary, touch points have been isolated for two-dimensional untrimmed flight with artificial aerodynamic data and trimmed flight with realistic aerodynamic data. These examples provide verifications of the touch point necessary conditions.

VIII. Three-Dimensional Extremals

Artificial Aerodynamic Data

The gimbal angle is set to zero ($\delta = 0$) for untrimmed three-dimensional flight, and the equations of motion described in Sec. IV are used. The time derivative of the inequality constraint is expressed as

$$\dot{S}(\boldsymbol{x}, \boldsymbol{u}) = -(1/2h_1)\rho V^3 \sin\gamma + \rho V[(1/m)\{T\cos\alpha - D - mg\sin\gamma\} + r\omega^2\cos\tau\{\cos\tau\sin\gamma - \sin\tau\cos\gamma\sin\psi\}] \tag{75}$$

As discussed in Sec. VI, the hodograph can be visualized in the (k_1–k_2–k_3) domain:

$$k_1 = T\cos\alpha - D \tag{76a}$$

$$k_2 = (T\sin\alpha + L)\cos\mu \tag{76b}$$

$$k_3 = (T\sin\alpha + L)\sin\mu \tag{76c}$$

Table 3 $\dot{S}_u$ vs q for three-dimensional flight with synthetic aerodynamic model

q_{max}, lb/ft^2	t_{en}, s	t_{ex}, s	Boundary arc, s	k_2	$\dot{S}_\alpha$
1001.0	68.676955232	68.677007083	5.19e−5	1.27781405e+6	−2.48110942e+1
970.0	68.515169477	68.581249171	6.61e−2	1.18825310e+6	−2.24162825e+1
850.0	67.839807813	67.997870103	1.58e−1	7.53253307e+5	−1.26185239e+1
750.0	67.198227379	67.217516087	1.93e−2	1.81006717e+5	−2.72052464e+0
727.9	67.022206058	67.022353342	1.47e−4	1.46444461e+4	−2.14731524e−1
727.55	67.019158882	67.019300702	1.42e−4	−1.43541848e+4	2.10393297e−1
727.5	67.018730036	67.018872103	1.42e−4	−1.43635866e+4	2.10519356e−1
727.0	67.014350171	67.014509015	1.59e−4	−1.51620343e+4	2.22097992e−1
720.0	66.950714525	66.954128366	3.41e−3	−6.85779870e+4	9.96767036e−1
700.0	66.735609674	66.792954332	5.73e−2	−2.61617581e+5	3.72056076e+0
600.0	63.366394770	67.065699269	3.70e+0	−1.41592459e+6	1.88420163e+1

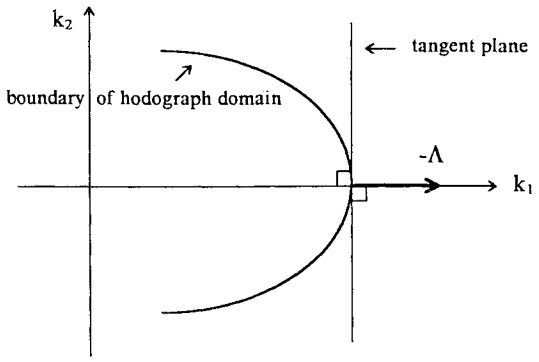

Fig. 3 Hodograph for the three-dimensional problem.

It has been shown that the hodograph is symmetric about the k_1 axis when the artificial aerodynamic data of Ref. 14 are used.

The regular optimal control problem was solved for a family of inequality constraint limits. The numerical data are shown in Table 3. It can be seen that when $q = 727.55$ lb/ft^2, the values of k_2 and $\partial\dot{S}/\partial\alpha$ change signs abruptly. The shortest boundary arc is about $1.42e{-}4$ s. Numerical results also show that λ_γ is zero, but λ_ψ is not zero on the shortest boundary arc.

It should be noted that a necessary condition for convexity of the hodograph in the $(k_1{-}k_2{-}k_3)$ system is that the maximum k_1 value is obtained at $k_2 = 0$ in the $(k_1{-}k_2)$ system. For a touch point to exist, Eq. (70) should be satisfied, i.e., $T\sin\alpha + (\partial D/\partial\alpha) = 0$. This means that α must be zero at a touch point. When $\alpha = 0$, then $T\sin\alpha + L = 0$, i.e., $k_2 = k_3 = 0$. Hence, at a touch point the state rate vector can be placed at the vertex of the hodograph in the $(k_1{-}k_2)$ system. Because the costate vector is perpendicular to the separating tangent plane at this point, the costate vector coincides with the k_1 axis, as shown in Fig. 3. This costate vector should be such that $\Lambda_{k_2}(\equiv \Lambda_\gamma) = 0$ and $\Lambda_{k_3}(\equiv \Lambda_\psi) = 0$. However, from the numerical results, it is clear that the touch point necessary conditions are not satisfied in this example.

Realistic Aerodynamic Data

In this section, extremal trajectories for three-dimensional flight are computed based on the realistic aerodynamic data. The differentiation of the inequality constraint, i.e., Eq. (54b), now contains the gimbal angle. For the three-dimensional trimmed flight, the touch point necessary condition requires that

$$T\sin(\alpha+\delta)\left(1+\frac{\partial\delta}{\partial\alpha}\right) + D_\alpha = 0 \qquad (77)$$

Equation (77) is only the condition that $k_1 = T\cos(\alpha+\delta) - D$ be maximized with respect to α at the touch point. As long as the aerodynamic data is smooth with respect to the angle of attack, the hodograph will be smooth. However, the convexity condition, $k_2 = k_3 = 0$ for maximum k_1, may not be satisfied in general and, hence, jump discontinuities in the velocity roll angle may be expected. Hence, the conditions for the existence at a touch point are not satisfied.

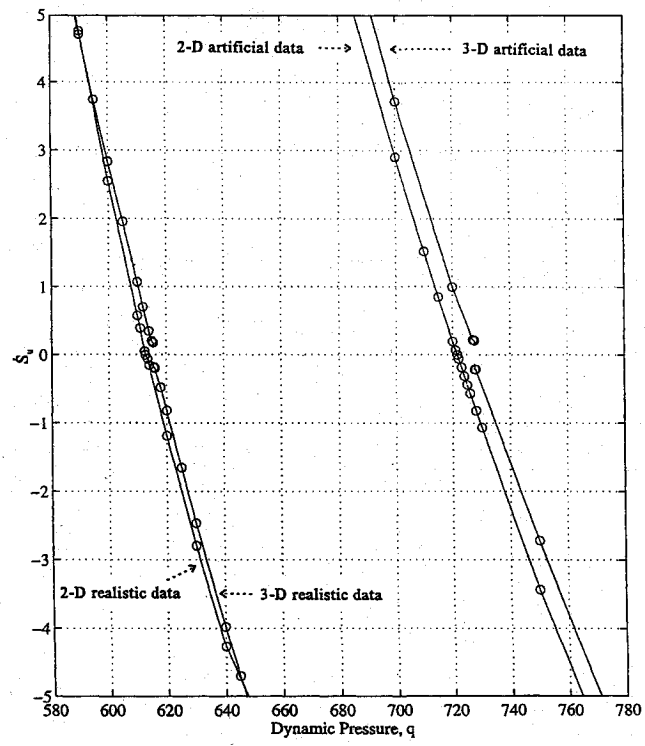

Fig. 4 $\dot{S}_u$ vs dynamic pressure q.

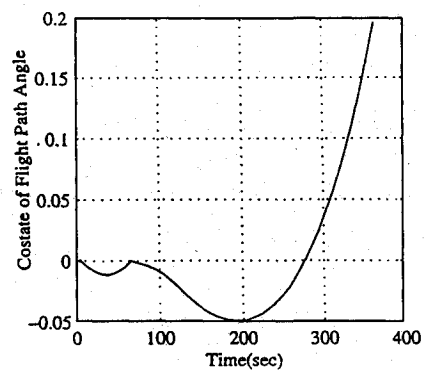

Fig. 5 Λ_γ history for the three-dimensional trajectory of the shortest boundary arc.

The trivial touch point ($\varepsilon_0 = 0$), corresponding to the unconstrained problem occurs at a dynamic pressure of 680 lb/ft^2. Table 4 shows that around a dynamic pressure of 615.547 or 615.548 lb/ft^2, the values of both k_2 and $\partial\dot{S}/\partial\alpha$ are discontinuous. The shortest boundary arc is about 7.60e−5 s. The value of $\partial\dot{S}/\partial\alpha$ is not zero for any dynamic pressure limit, and the value of k_1 in the hodograph is not an extremum for $k_2 = 0$. Using both the artificial and realistic aerodynamic data, Fig. 4 shows that $\partial\dot{S}/\partial\alpha$ is discontinuous for

Table 4 $\dot{S}_u$ vs q for three-dimensional flight with realistic aerodynamic model

q_{max}, lb/ft^2	t_{en}, s	t_{ex}, s	Boundary arc, s	k_2	$\dot{S}_\alpha$
679.9	67.861908212	67.861965375	5.72e−5	5.12379541e+5	−8.20266 670e+0
650.0	66.968098700	66.993860958	2.58e−2	3.03063745e+5	−5.40106436e+0
620.0	66.031037203	66.032484567	1.45e−3	3.88172846e+4	−8.15124748e−1
616.0	65.899519051	65.899611664	9.26e−5	3.21108756e+3	−1.96908113e−1
615.6	65.886369830	65.886446335	7.65e−5	2.16710468e+3	−1.78275835e−1
615.546	65.884545389	65.884621378	7.60e−5	−1.85603040e+4	1.77974785e−1
615.5	65.883083678	65.883160301	7.66e−5	−1.85814523e+4	1.78406797e−1
615.0	65.866719920	65.866823842	1.04e−4	−2.01765645e+4	2.06607457e−1
610.0	65.692453339	65.695594241	3.14e−3	−6.99722050e+4	1.07143992e+0
600.0	65.281699248	65.308560112	2.69e−2	−1.71240900e+5	2.83613121e+0
570.0	63.793817307	64.296448421	5.03e−1	−5.43568788e+5	9.32604498e+0

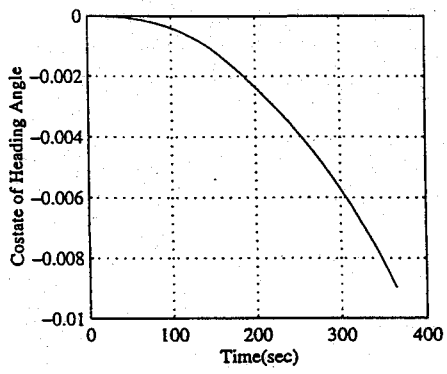

Fig. 6 Λ_Ψ history for the three-dimensional trajectory of the shortest boundary arc.

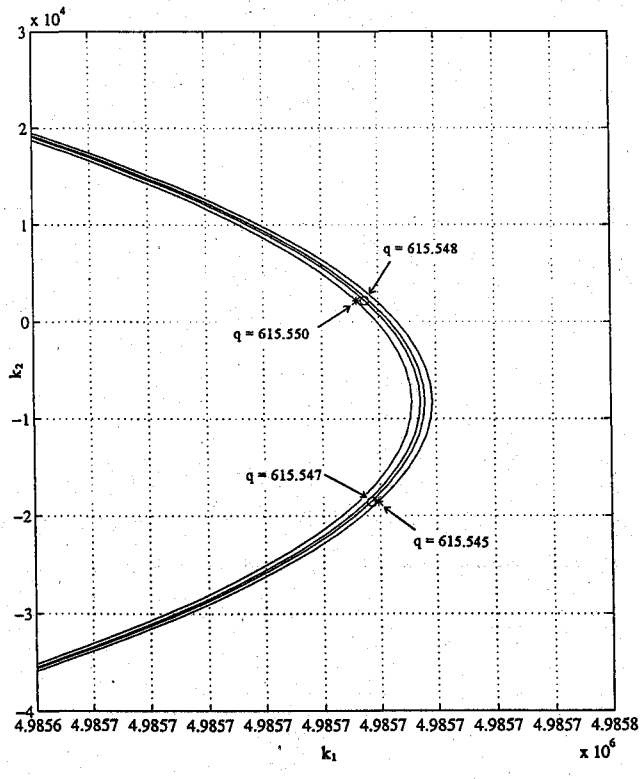

Fig. 7 Discontinuity in hodographs of the three-dimensional problem at the entry points.

the three-dimensional trajectories, whereas it is continuous for the two-dimensional trajectories. The numerical results show that, for the three-dimensional trajectories, the costate of flight path angle is zero, but the costate of heading angle is not zero even on the shortest boundary arc (Figs. 5 and 6). Figure 7 shows the jump in the entry point conditions on the hodograph near the dynamic pressures corresponding to the shortest boundary arc. Figure 7 shows that the state rate vector cannot be placed at the vertex of the hodograph. This study verifies that touch points do not occur in three-dimensional ascent trajectories.

IX. Conclusions

For the first time, examples are presented of optimal ascent trajectories with first-order state variable inequality constraints, which show the existence of touch points. It was shown that touch points can occur in extremal two-dimensional ascent flight. However, they could not be found in the more general three-dimensional flight. The family of inequality constraints were parameterized by the dynamic pressure limit. The necessary conditions for a touch point to occur in connection with a first-order inequality constraint were reviewed. Additional insights into the nature of the Lagrange multipliers at touch points were inferred by making use of the hodograph analysis.

Acknowledgment

We thank Hans Seywald of Analytical Mechanics Associates for many illuminating discussions, in particular in regard to the "Hodograph Analysis" section.

References

[1]Bryson, A. E., Denham, W. F., and Dreyfus, S. E., "Optimal Programming Problems with Inequality Constraint, I: Necessary Conditions for Extremal Solutions," *AIAA Journal*, Vol. 1, No. 11, 1963, pp. 2544–2550.

[2]Speyer, J. L., and Bryson, A. E., "Optimal Programming Problems with a Bounded State Space," *AIAA Journal*, Vol. 6, No. 8, 1968, pp. 1488–1491.

[3]Jacobson, D. H., Lele, M. M., and Speyer, J. L., "New Necessary Conditions of Optimality for Control Problems with State-Variable Inequality Constraints," *Journal of Mathematical Analysis and Applications*, Vol. 35, 1971, pp. 255–284.

[4]Kreindler, E., "Additional Necessary Conditions for Optimal Control with State-Variable Inequality Constraints," *Journal of Optimization Theory and Applications*, Vol. 38, No. 2, 1982, pp. 241–250.

[5]Maurer, H., "On Optimal Control Problems with Bounded State Variables and Control Appearing Linearly," *SIAM Journal on Control and Optimization*, Vol. 15, No. 3, 1977, pp. 345–362.

[6]Maurer, H., and Gillessen, W., "Application of Multiple Shooting to the Numerical Solution of Optimal Control Problems with Bounded State Variables," *Computing*, Vol. 15, 1975, pp. 105–126.

[7]Norris, D. O., "Nonlinear Programming Applied to State-Constrained Optimization Problems," *Journal of Mathematical Analysis and Applications*, Vol. 43, 1973, pp. 261–272.

[8]Seywald, H., and Cliff, E. M., "On the Existence of Touch Points for First-Order State Inequality Constraints," AIAA Paper 93-3743, Aug. 1993.

[9]Kirk, D. E., *Optimal Control Theory: An Introduction*, Prentice–Hall, Englewood Cliffs, NJ, pp. 227–234.

[10]McIntyre, J., and Paiewonsky, B., "On Optimal Control with Bounded State Variables," *Advances in Control Systems*, edited by C. T. Leondes, Vol. 5, 1967, pp. 389–419.

[11]Shaver, D. A., and Hull, D. G., "Advanced Launch System Trajectory Optimization Using Suboptimal Control," AIAA Paper 90-3413, Aug. 1990.

[12]Seywald, H., and Cliff, E. M., "A Feedback Control for the Advanced Launch System," AIAA Paper 92-2619, Aug. 1992.

[13]Cliff, E. M., Seywald, H., and Bless, R. R., "Hodograph Analysis in Aircraft Trajectory Optimization," AIAA Paper 93-3742, Aug. 1993.

[14]Bless, R. R., Hodges, D. H., and Seywald, H., "State-Constrained Booster Trajectory Solutions Via Finite Elements and Shooting," AIAA Paper 93-3747, Aug. 1993.